Potential role of the quasi-biennial oscillation in the stratosphere-troposphere exchange as found in water vapor in general circulation model experiments

Marco A. Giorgetta and Lennart Bengtsson

Max-Planck-Institute for Meteorology, Hamburg, Germany

Abstract. The tropical tropopause is considered to be the main region of upward transport of tropospheric air carrying water vapor and other tracers to the tropical stratosphere. The lower tropical stratosphere is also the region where the quasi-biennial oscillation (QBO) in the zonal wind is observed. The QBO is positioned in the region where the upward transport of tropospheric tracers to the overworld takes place. Hence the QBO can in principle modulate these transports by its secondary meridional circulation. This modulation is investigated in this study by an analysis of general circulation model (GCM) experiments with an assimilated QBO. The experiments show, first, that the temperature signal of the QBO modifies the specific humidity in the air transported upward and, second, that the secondary meridional circulation modulates the velocity of the upward transport. Thus during the eastward phase of the QBO the upward moving air is moister and the upward velocity is less than during the westward phase of the QBO. It was further found that the QBO period is too short to allow an equilibration of the moisture in the QBO region. This causes a QBO signal of the moisture which is considerably smaller than what could be obtained in the limiting case of indefinitely long QBO phases. This also allows a high sensitivity of the mean moisture over a QBO cycle to the El Niño-Southern Oscillation (ENSO) phenomena or major tropical volcanic eruptions. The interplay of sporadic volcanic eruptions, ENSO, and QBO can produce low-frequency variability in the water vapor content of the tropical stratosphere, which renders the isolation of the QBO signal in observational data of water vapor in the equatorial lower stratosphere difficult.

1. Introduction

The stratosphere-troposphere exchange (STE) has recently become a strongly discussed subject, especially in the context of tracer transport between the troposphere and the middle atmosphere, which is relevant for the understanding of photochemistry. A recent review article of this subject is given by *Holton et al.* [1995]. Further, the new satellite measurements of middle atmosphere tracer mixing ratios, for example, of H_2O by the Halogen Occultation Experiment (HALOE) and the microwave limb sounder (MLS) on the Upper Atmosphere Research Satellite (UARS), allow validation of transport processes which was hardly possible before (reviewed by, e.g., *Dessler et al.* [1998]).

One specific issue is the exchange at the tropical tropopause. The tropical tropopause is assumed to be a surface across which tracers in general pass upward. However, if the tracer concentration at this separating surface is subject to a modulation in time, one may expect to find the same modulation in time at higher levels with a time lag depending on the vertical transport velocity between the tropopause and this higher level, provided that the lateral mixing to the subtropics and vertical mixing are sufficiently small. This mechanism was suggested already by *Kley et al.* [1979], based on balloon measurements of the specific humidity in the lower stratosphere, and was recently named the atmospheric tape recorder by *Mote et al.* [1996]. They validated this effect for water vapor measured by MLS and HALOE, showing that air transported upward retains a memory for tropical tropopause conditions for at least 18 months, since the tropical lower stratosphere is indeed well isolated toward the subtropical latitudes.

This modulation of water vapor at the tropical tropopause is related to the ambient temperature limiting the mixing ratio of water vapor passing through this level. It is not yet understood exactly how the water vapor is passed upward, since the zonally or monthly averaged tropopause temperature would allow higher water vapor contents passing upward. This suggests that water vapor is normally passing some areas colder than the average, like, for example, in the warm pool region where tropopause temperatures can reach values low enough to explain the very low water vapor mixing ratios found in the lower tropical troposphere [*Newell*

and Gould-Stewart, 1981]. Nevertheless, it is still a difficult task to identify such cold traps as discussed by *Mote et al.* [1996]. However, the observations confirm in general the picture of the atmospheric tape recorder, and there is observational evidence for a quasi-biennial oscillation (QBO) induced variation of the recorder winding speed [*Randel et al.,* 1998]. Further, this variation was corroborated by *Mote et al.* [1996] with a two-dimensional mechanistic model, whose only source of interannual variability was a parameterized QBO. The QBO influence on the tropical meridional and vertical circulation also generates signals in constituent distributions in areas of significant meridional or vertical gradients of the constituent fields. QBO signals have been detected also in O_3, CH_4, and HF [*Cordero et al.,* 1997; *Randel and Wu,* 1996; *Randel et al.,* 1998; *Tung and Yang,* 1994].

This study here presents results of general circulation model (GCM) integrations concerning QBO-induced signals not only in the vertical velocity, but also in the water vapor content in the lower equatorial stratosphere. The former is caused directly by the secondary circulation forced by the QBO, while the latter is an indirect effect due to the temperature changes at the equatorial tropopause, which is caused by the adiabatic vertical motion of the secondary circulation of the QBO. The paper is structured as follows. Section 2 presents the experiments used for this analysis. Section 3 describes the assimilation method by which the QBO was generated in the GCM. Section 4 discusses some systematic deficiencies of the model. Section 5 presents results, first from experiments with steady state QBO phase states and climatological sea surface temperature (SST) fields, and second from experiments with assimilated QBO and prescribed SST following observations. Section 6 concludes this study.

2. Experimental Design

The analyzed data come from a set of GCM experiments which were designed to investigate the importance of the QBO for the tropospheric circulation and some aspects of the dynamics in the QBO domain itself. These experiments were based on the comprehensive ECHAM4 general circulation model [*Roeckner et al.,* 1996]. The ECHAM4 model is a spectral general circulation model. It is used in its standard resolution; that is, the dynamics is computed at a triangular truncation at wave number 42, while the physical parameterizations are calculated on the associated Gaussian grid at a grid resolution of about 2.8°. The model contains 19 layers extending from the surface to 10 hPa, where the upper four layers at 70, 50, 30, and 10 hPa are entirely in the lower stratosphere. The model is based on the primitive equations. Prognostic variables are vorticity, divergence, temperature, logarithm of surface pressure, specific humidity and total cloud water (combining liquid and ice phase). The first four components are represented in spectral space, while the last two components are represented on the Gaussian grid. The transport of specific humidity and total cloud water is calculated by a semi-Lagrangian scheme developed by *Williamson and Rasch* [1994]. The model com-

prises many physical parameterizations, whereof the following are directly relevant for water vapor sinks, sources, and transport.

The vertical diffusion of momentum, heat, moisture, and cloud water is computed in a high-order closure scheme depending on the turbulent kinetic energy [*Brinkop and Roeckner,* 1995]. Horizontal diffusion is expressed in the form of a hyper-Laplacian ∇^{2q} with $2q = 10$ in the troposphere, which essentially confines the damping to the high-wavenumber end of the spectrum. To avoid fictitious reflection at the upper boundary, a high-diffusion sponge zone is realized through a gradual decrease of the order of the scheme in the lower stratosphere. The diffusion operator is applied to vorticity, divergence, and temperature but not to the water components which are advected by the semi-Lagrangian scheme.

Gravity wave drag associated with orographic gravity waves is simulated after *Miller et al.* [1989], using directionally dependent subgrid-scale orographic variances obtained from a high-resolution U.S. Navy data set. Cumulus convection distinguishes shallow, midlevel, and deep convection, based on a bulk mass flux concept of *Tiedtke* [1989] and modified according to *Nordeng* [1996] to calculate organized entrainment as a function of buoyancy instead of moisture convergence. The buoyancy calculation also considers the water loading. The organized detrainment is calculated for a spectrum of clouds of different depths, using an adjustment closure for deep convection. Cloud water detrained at cloud tops provides a source term for stratiform clouds. Stratiform cloud water content is computed in budget equations following *Sundquist* [1978]. Fractional cloud cover is parameterized as a function of mean relative humidity [*Sundquist et al.,* 1989]. The liquid and ice phases are split empirically [*Rockel et al.,* 1991]. The radiation scheme is a modified version of the European Centre for Medium-Range Weather Forecasts (ECMWF) scheme [*Fouquart and Bonnel,* 1989; *Morcrette et al.,* 1986]. The single scattering properties of cloud droplets and ice crystals are derived from Mie theory [*Rockel et al.,* 1991], and the effective radii of droplets and ice crystals follow *Roeckner* [1995].

Because of the low top at 10 hPa and coarse vertical resolution, it is not surprising that the QBO is not simulated by the model itself. However, this limitation can be circumvented by carrying out integrations with an assimilated QBO, thus allowing external control on the phase state of the QBO and its phase relationship to the annual cycle. Considering this, five experiments were designed as follows:

1. CONTROL is the basic experiment, that is, an integration of the unmodified GCM. The model is run over 10 years with climatological SST fields at the lower boundary. There is no QBO in this experiment. The equatorial zonal winds in the lower stratosphere are weak easterlies.

2. W-QBO differs from CONTROL by the assimilation of the QBO in a perpetual eastward phase state. The equatorial zonal winds are westerlies at 30, 50, and 70 hPa, but easterlies at 10 hPa.

3. E-QBO differs from CONTROL by the assimilation of the QBO in a perpetual westward phase state. The equa-

Table 1. Schematic Arrangement of the Experiments With Respect to SST Forcing (Rows) and QBO Assimilation (Columns)

	No QBO	Westerly QBO	Easterly QBO	Observed QBO
Climatological SST	CONTROL	W-QBO	E-QBO	· · ·
Observed SST	AMIP	· · ·	· · ·	AMIP-QBO

SST denotes sea surface temperature; QBO denotes quasi-biennial oscillation.

torial zonal winds are easterlies at 30, 50, and 70 hPa, but westerlies at 10 hPa.

4. AMIP differs from CONTROL by the prescription of observed SST fields instead of climatological SST fields. The integration was run for SST fields from January 1979 to December 1992, that is, over 14 years.

5. AMIP-QBO differs from AMIP by the assimilation of the QBO for the same years as the SST. The phase of the QBO follows the monthly mean observations in Singapore.

The experiments W-QBO and E-QBO serve to detect QBO signals in the circulation, either by statistical methods or by the examination of hypothetical mechanisms. The prescription of constant QBO phases combined with the prescription of climatological SST fields facilitates such investigations because of the reduction of the variance. The experiments CONTROL, AMIP, and AMIP-QBO represent a set of experiments with increasing variance. The variability in CONTROL is generated internally. In AMIP it is strengthened externally by the prescribed El Niño-Southern Oscillation (ENSO). AMIP-QBO has the highest variability due to the additional assimilation of the QBO. AMIP and AMIP-QBO serve to recover QBO signals under more realistic conditions as given by the prescribed SST, present in both experiments, and the realistically evolving QBO in AMIP-QBO. Table 1 shows schematically the experiments according to the SST forcing and the QBO assimilation.

3. Assimilation of the QBO

The assimilation procedure is based on *Krishnamurti et al.* [1990] and is realized by a local and linear relaxation of the zonal wind in the QBO domain to a zonally uniform artificial QBO. This artificial QBO is constructed as an equatorial jet with a Gaussian profile in the meridional direction and a prescribed equatorial vertical wind profile, as compiled by *Pawson et al.* [1993]. The half width of the Gaussian profile varies from 10°latitude at 70 hPa to 15°at 10 hPa. The vertical zonal wind profile data set contains essentially profiles measured at Singapore station. The assumptions of zonal symmetry and Gaussian meridional shape are well justified, following analyses by *Dunkerton and Delisi* [1985] and *Naujokat* [1986] with respect to equatorial station data. Also, *Pawson and Fiorino* [1998b] state that the Singapore profiles are representative of the zonal means in the reanalysis.

The relaxation timescale was selected as short as necessary to get a reasonably realistic QBO, and as long as possible, in order not to disturb the model dynamics more than necessary. This allows the model to develop its dynamics within the QBO domain on timescales shorter than the relaxation timescale. This is set uniformly to 10 days between 10°N and 10°S at 50 hPa and higher. Poleward of this band the reciprocal value of the relaxation timescale decreases linearly to zero at 20°latitude. At 70 hPa the assimilation at a given latitude is half as strong as on higher levels at the same latitude. The zonal wind remains unaffected by the assimilation at 100 hPa and at latitudes poleward of 20°. The QBO has been assimilated in a similar way in, for example, the works by *Kodera et al.* [1991], *Hamilton* [1995], and *Balachandran and Rind* [1995].

The result of this assimilation procedure in AMIP-QBO is shown together with the observed zonal wind field in Figure 1. A comparison of the observed and assimilated QBO shows a general correspondence of the phase state. The amplitudes of the assimilated westerlies and easterlies reach typically 75% of the prescribed values. The QBOs obtained in AMIP-QBO, like the steady state QBO phases in W-QBO and E-QBO, are realistic enough to force the GCM to generate a secondary circulation in the meridional plane.

The secondary meridional circulation causes a well-defined temperature signal in the QBO domain. This is due to the Coriolis effect (near equator: $f = \beta \times y$) which forces meridional convergence and divergence in the eastward and westward phase of the QBO, respectively, thus creating vertical divergence (eastward jet) and convergence (westward jet). Descending motion, hence adiabatic warming, occurs below the eastward jet axis and above the westward jet. Ascending motion, hence adiabatic cooling, occurs above the eastward jet axis and below the westward jet. This signal is strong in the center of the domain, but also present at the lowermost stratospheric levels. Thus the QBO may modulate the temperature also at the tropical tropopause, that is, lead to a relative warming (cooling) at the equator and to the opposite signal in the subtropics when the QBO is in its eastward (westward) phase.

Dunkerton and Delisi [1985] determined an equivalent temperature amplitude of the QBO, based on radiosonde measurements. They found values of 3 to 3.5 K for the temperature oscillation at 30 hPa in equatorial latitudes. The computation of the same quantity in AMIP-QBO gives a value of 3.4 K at the equator (Figure 2).
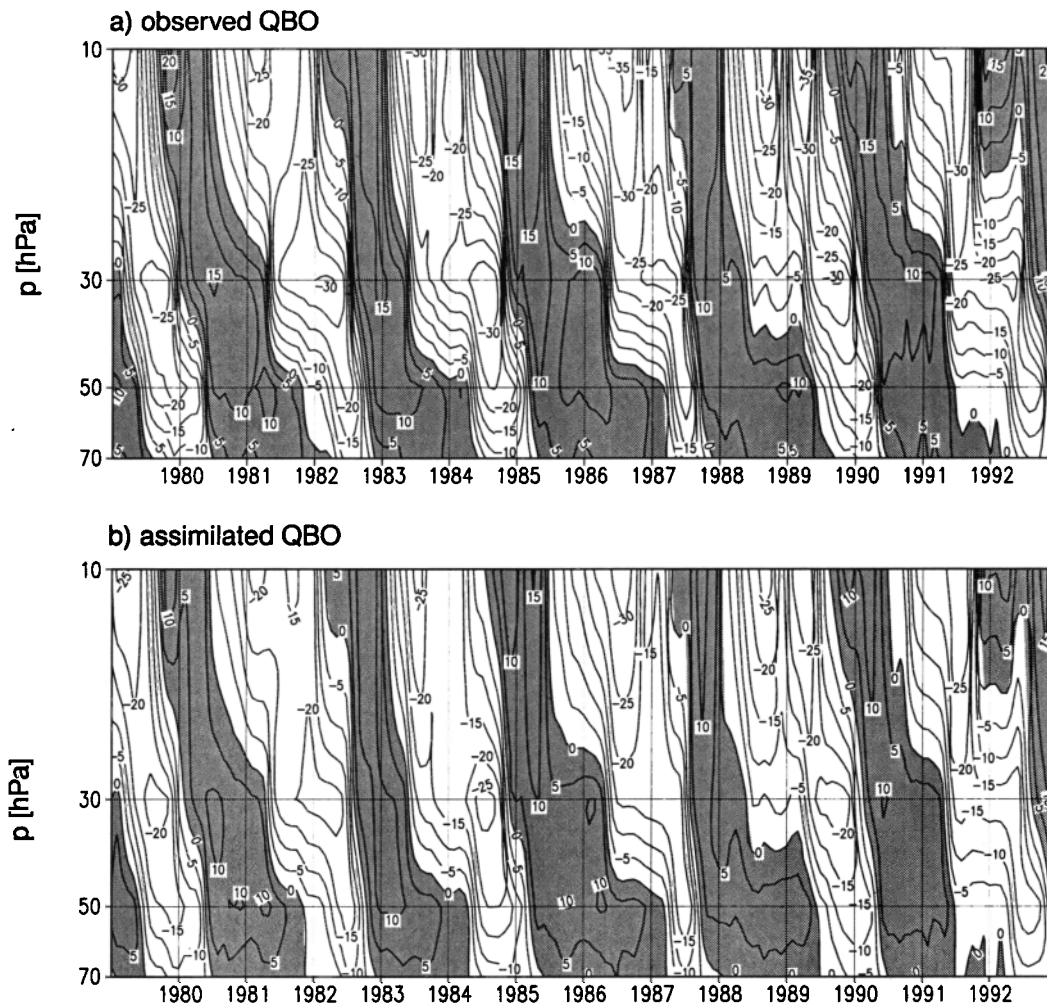
Figure 1. Zonal mean zonal wind (m/s) at the equator between 70 to 10 hPa (a) as observed in Singapore and (b) as obtained in AMIP-QBO. Westerlies are shaded.
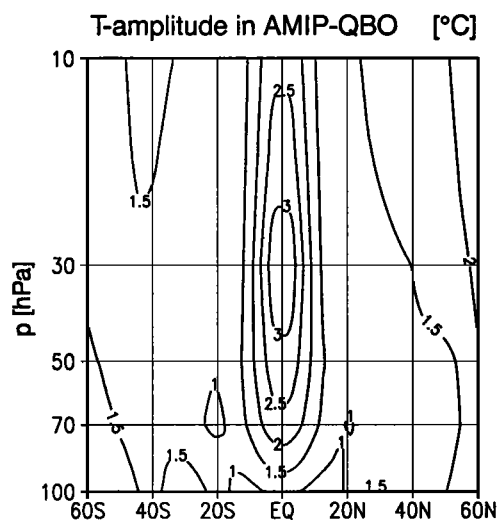

Figure 2. Equivalent amplitude of QBO-induced zonal mean temperature in AMIP-QBO.

4. Model Bias in the Stratospheric Circulation and in the Specific Humidity

As pointed out earlier, this set of experiments was carried out originally to study tropospheric QBO signals, hence the use of a tropospheric GCM. It is, of course, questionable whether it is worthwhile to investigate the STE in a model where only the lower stratosphere is resolved, and therefore this has to be justified. Critical points are the tropical tropopause temperature which limits the upward specific moisture transfer, and the midlatitude wave driving in the middle atmosphere. This wave driving is important not only for the zonal wind structure in the stratosphere, but also for the stratospheric uptake of tropical tropospheric air [*Holton et al.*, 1995]. Therefore annual cycles of temperature, zonal wind and the transformed Eulerian mean stream function are compared in ECHAM4 as used for this study, and the ECMWF reanalysis (ERA) [*Gibson et al.*, 1997] and National Centers for Environmental Prediction (NCEP) reanalysis [*Kalnay et al.*, 1996].

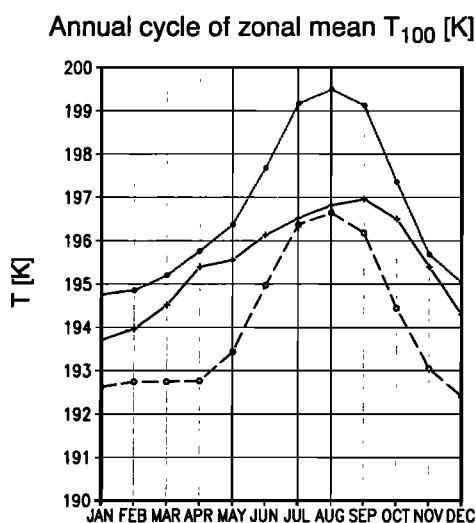## Annual cycle of zonal mean T$_{100}$ [K]

Figure 3. Climatological annual cycle of zonal mean temperature at the equator at 100 hPa for ECHAM4 CONTROL (short-dashed curve), ECMWF reanalyses 1979-1992 (solid curve), and NCEP reanalyses 1979-1992 (long-dashed curve).

4.1. Temperature at the Tropical Tropopause

A comparison of ECHAM4-CONTROL, NCEP, and ERA temperature profiles shows all three data sets contain the tropical tropopause in the layer centered at 100 hPa. The annual and zonal mean temperature at 100 hPa at the equator is 195.5 K in CONTROL, 194.1 K in ERA, and 196.7 K in NCEP, where the reanalyses data have been averaged over the years 1979 to 1992. The ECHAM4 value is almost in the middle of the range given by ERA and NCEP (cf. *Pawson and Fiorino* [1998a] for a detailed discussion of the tropical thermal structure in ERA and NCEP). The annual cycle of the temperature at 100 hPa at the equator is shown in Figure 3. The ERA annual cycle attains a minimum in December and stays on a similar level until April. Later, the temperature increases strongly to a maximum in August. Then the temperature drops at a comparable rate until December. The

total range is 4.0 K. The NCEP minimum is approximately 2 K higher than in ERA and occurs in January. The temperature increases as early as in the spring months and peaks in August 4.7 K above the minimum value, followed by a decrease. Both reanalyses differ mainly in the minimum value, in the rate of warming in the months February to April, and in the range; otherwise, both curves are similar. The model minimum also occurs in January, at a value between both reanalyses. The following increase in spring is, however, 50% stronger than in NCEP. This is followed by a comparatively weaker rate of warming until September, peaking 3.3 K higher then the minimum. Thus the magnitude of the model annual cycle is 0.7 K and 1.4 K smaller than ERA and NCEP, respectively, but the cycle stays in the bounds given by ERA and NCEP. The modeled annual cycle is presumably too flat during summer, but the minimum temperature is reasonable. For the relevance of gridded 100 hPa temperature for the cold trap problem, the reader is referred to the extensive discussion in the works by *Mote et al.* [1996].

4.2. Extratropical Zonal Winds in the Lower Stratosphere

The uppermost layer of the tropospheric general circulation model ECHAM4 is centered at 10 hPa, that is, the model domain contains only the troposphere and the lower stratosphere. The tropical lower stratosphere is represented by four layers only, centered at 10, 30, 50, and 70 hPa, followed by layers at approximately 110, 150, and 200 hPa. Further, these layers are exposed to an increased horizontal diffusion of momentum and temperature, as stated above. Thus it is likely that the planetary wave activity in the surrogate stratosphere of the model is biased, having implications for the strength, position and hemispheric asymmetry of the extratropical zonal wind structure and implicitly for the meridional residual circulation.

Figure 4 shows the annual cycle of the climatological zonal mean zonal wind at 50 hPa, as found in the model and in both reanalyses data sets. The Southern Hemisphere (SH) jet has a very similar maximum strength of approximately
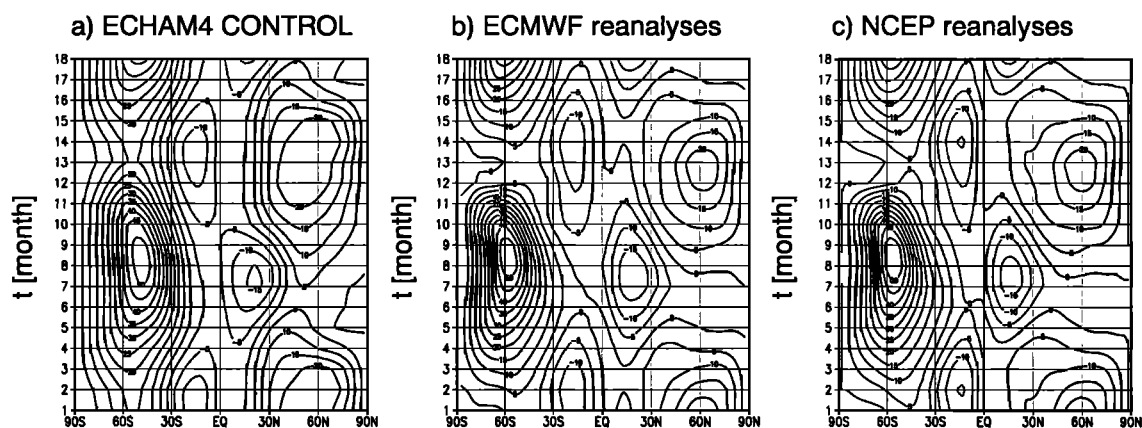

Figure 4. Climatological annual cycle of zonal mean zonal wind at 50 hPa in (a) ECHAM4 CONTROL, (b) ECMWF reanalyses 1979-1992, and (c) NCEP reanalyses 1979-1992. The isoline distance is 5 m/s.
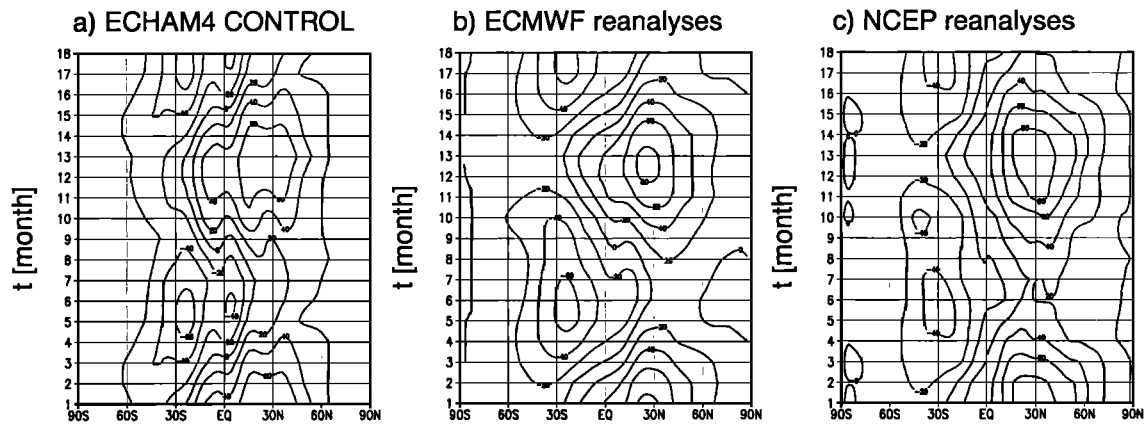
Figure 5. Climatological annual cycle of transformed Eulerian mean stream function at 70 hPa in (a) ECHAM4 CONTROL, (b) ECMWF reanalyses 1979-1992, and (c) NCEP reanalyses 1979-1992. The isoline distance is 30×10^8 kg/s.

52 m/s in all three data sets, though the modeled maximum is approximately 7°closer to the equator. The maximum is found in August/September in all cases. The breakdown of the SH jet from October to December is very similar in both reanalyses, but is clearly weaker in the model, where the zonal mean zonal wind near 60°S never falls below 15 m/s. This is an indication of an underestimated wave activity in the model during this season. The SH winter circulation is essentially zonal, that is, hardly influenced by wave activity, hence the good agreement of the modeled maximum zonal wind in SH winter with reanalyses. In the Northern Hemisphere (NH), both reanalysis are again in good agreement with respect to the westerlies, which obtain a maximum value of 23 m/s in December/January. In the model the westerlies reach 24 m/s, only slightly stronger than the reanalyses, but these westerlies extend over a larger latitude range southward and last for a longer time. This bias is explained again by an underestimated wave activity, which affects the winter as well as the spring season in the NH. The much lower maximal zonal wind in the NH compared to the SH is a result of the stronger NH wave activity. This asymmetry is well captured by the model. Thus it is likely that this model suffers in general from a lack of wave activity, especially along 30°latitude. The subtropical easterlies are comparable in position and strength among all three data sets. In general, the strength and the timing of the maxima of the zonal mean westerlies are fairly realistic compared to reanalyses, and the major discrepancies are found in the more equatorward position and the mentioned lack of wave activity.

4.3. Transformed Eulerian Mean Stream Function

The upward mass transport above the tropical troposphere is strongly influenced by nonlocal wave activity in the middle atmosphere as described in the framework of the "downward control principle" [*Haynes et al.*, 1991]. Rossby wave and gravity wave activity acting on the westerly jets cause at the same time a meridional residual circulation, taking air from the region above the tropical tropopause up to the "overworld". This uptake may be estimated by comput-

ing the transformed Eulerian mean (TEM) stream function of model and reanalyses at 70 hPa, which is close to the boundary to the overworld [*Rosenlof et al.*, 1997]. This was done based on the resolved circulation fields of all three data sets by integrating v* from the uppermost level downward to 70 hPa [cf. *Andrews et al.*, 1987]. Figure 5 shows the obtained climatological annual cycle. The absolute value of the minimum near 30°S in May and the maximum near 30N in January represent the downwelling across the 70 hPa level poleward of the respective latitude. The modeled minimum of -70×10^8 kg/s and maximum of 80×10^8 kg/s are similar to values of -67×10^8 kg/s and 84×10^8 kg/s in ERA. The NCEP reanalysis contains a stronger maximum of 92×10^8 kg/s and a weaker and long-lasting negative band reaching just -50×10^8 kg/s. The tropical upwelling across 70 hPa in January, computed as the difference of the maximum and minimum values of the mass stream function, takes values of 108.1×10^8 kg/s (ECHAM4), 96.6×10^8 kg/s (ERA) and 107.1×10^8 kg/s (NCEP). The ECHAM4 value is comparable to the NCEP value. In June the upwelling attains values of 89.0×10^8 kg/s (ECHAM4), 75.9×10^8 kg/s (ERA) and 71.6×10^8 kg/s (NCEP). Here the modelled upwelling is overestimated by approximately 20% with respect to the reanalyses values. However, in all cases there occurs a clear seasonal cycle in the tropical upwelling with stronger upwelling in boreal winter than in austral winter, as expected from the different intensity of the wave mean flow interaction in the Northern and Southern hemispheres.

4.4. Stratospheric Moisture

The GCM used for the experiments has a systematic error in the water vapor content in the stratosphere, as is shown in Figure 6. The left panel shows the time average of HALOE measurements of H_2O volume mixing ratio from January 1993 to December 1997 and the right panel shows the annual climatological mean of the same quantity in the experiment AMIP-QBO.

First, there is a qualitative difference in the vertical and horizontal structure of the fields. The observed field has a minimum at the equator at 70 hPa. The humidity generally
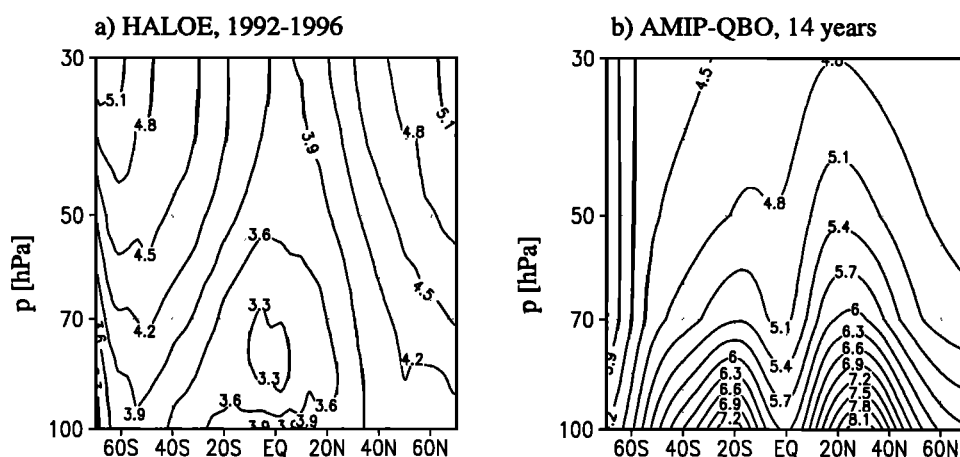
Figure 6. Water vapor content in ppmv in (a) as observed by the Halogen Occultation Experiment (HALOE) in the years 1992 to 1997 and (b) as obtained in the experiment AMIP- QBO, averaged over 14 years.

increases toward higher levels and latitudes. The main reason for this structure is the methane oxidation process, which provides a water vapor source in the real middle atmosphere, generating approximately $2H_2O$ for each CH_4. This source term is small at levels below approximately z=30 km, but increases the water vapor loading of originally tropical air parcels significantly as they are lifted upward and later poleward [Mote et al., 1996; Randel et al., 1998]. The methane oxidation process creates air of nearly constant mixing ratio of $2CH_4 + H_2O$ in the complete stratosphere, except in the SH polar vortex (due to desiccation) and in the equatorial upwelling region (where the air has not yet been processed) [Randel et al., 1998]. This explains the observed increase of the observed specific humidity toward higher levels and higher latitudes, where parcels have been exposed to methane oxidation over some period. The modeled field shows an equatorial minimum too. However, the humidity decreases strictly with height, though the vertical gradient decreases strongly above 50 hPa. The primary reason for this monotonicity is the missing methane oxidation, which is not considered in this GCM. The model creates upward fluxes of relatively dry air near the equator and comparatively moist air near 20°S and 25°N. The resulting tropical meridional gradients decrease with height, as the air masses are mixed more and more.

Second, there is a quantitative problem, inasmuch as the equatorial volume mixing ratio in the model is considerably above the observed values. At 100 hPa the mixing ratio is exceeded by 2 ppmv at the equator. A bias of this kind has to be expected due to the resolved scales of this GCM, which are 2.8°in the horizontal and 2 km in the vertical direction around the tropopause. This overestimation happens even though the modeled equatorial temperature is in a reasonable range with respect to the reanalyses data. Gridded data, however, are in general too high to explain the very low moisture values of the lower tropical stratosphere [Newell and Gould-Stewart, 1981; Mote et al., 1996]. As the model computes the saturation pressure depending on the representative tem-

perature for a grid cell, there occurs necessarily a positive bias with respect to nature, where upwelling air seems to originate from colder than normal areas.

Nevertheless, the model is able to set up a clear climatological annual cycle in the stratospheric humidity. Figure 7a shows the zonal mean humidity at the equator, Figure 7b the deviation of the zonal mean annual cycle from the annual mean. At 100 hPa the minimum and maximum occur in January and September, respectively, in agreement with the occurrence of the minimum and maximum temperature (Figure 3). The absolute minimum in moisture is created at 70 hPa in February. Positive and negative anomalies propagate upward (Figure 7b), demonstrating the principal ability of this model to create the signature of the atmospheric tape recorder. The ascent rate, however, is greater than observed. Mote et al. found transit times of 6 months or more for the ascent from 100 hPa to 46 hPa, while the modeled ascent from 100 hPa to 50 hPa takes only 2 months, which is clearly too fast. This error is also related to the insufficient vertical resolution.

The preceding sections have shown biases of the GCM with respect to reanalyses data or satellite data. It is found that the circulation in the resolved stratosphere is acceptable in terms of strength of the jets at 50 hPa and their hemispheric asymmetry. The tropical upwelling across the 70 hPa level has the correct seasonality, but is probably too strong in boreal summer. In general, the TEM stream function is acceptable too. From a quantitative point of view, both fields have deficiencies indicative of underestimated wave action, especially equatorward of the jets. With respect to stratospheric water vapor, the model generates a latitudinal minimum in the specific humidity in the equatorial latitudes, as also found in observations. This minimum is only explicable by the low temperatures prevailing at the equatorial tropopause, that is, the temperature field is the main constraint to the humidity. Major differences occur due to the missing simulation of methane oxidation. Further deficiencies occur due to an exaggerated upward flux of moisture
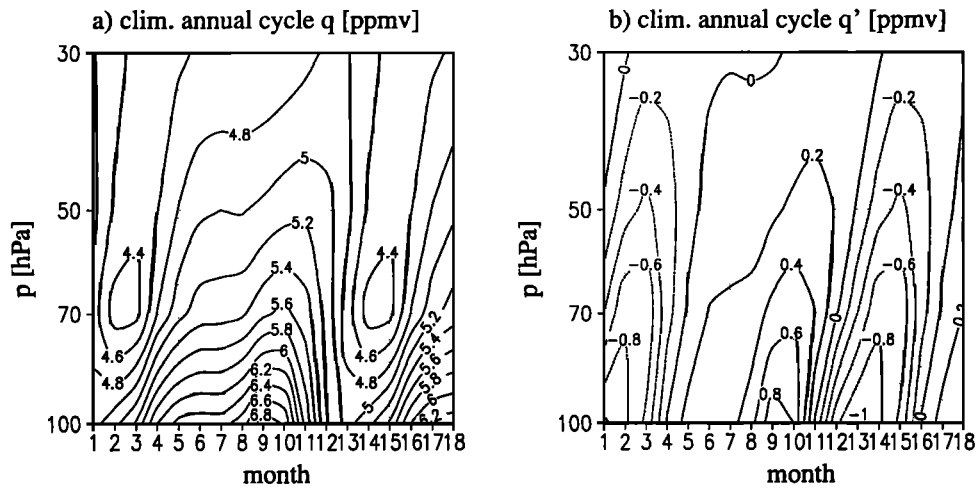
Figure 7. (a) Climatological annual cycle of moisture q at the equator and (b) deviation q' from climatological annual mean in ppmv.

near 20°S and 25°N, resulting from the coarse vertical resolution. Additionally, the model is able to propagate the equatorial moisture anomalies upward, although too fast.

The following investigation is primarily directed at the interannual variation of the water vapor content in the equatorial stratosphere due to the QBO, which is mainly a result of a QBO induced modulation of the tropopause temperature as shown below. The temperature limitation to equatorial tropopause humidity is clearly seen in the model. Hence this GCM allows one, in conjunction with the experimental design, to obtain insight into the potential deviation of stratospheric water vapor uptake explained by the QBO with respect to the undisturbed annual cycle in the equatorial latitudes.

5. Results

5.1. Perpetual QBO Phases

This section presents results obtained from the experiments CONTROL, W-QBO, and E-QBO, which have a low

tropical variance since there was no interannual SST variation. Both QBO experiments were run in the limiting case of perpetual and opposite QBO phases; hence they differ systematically in the zonal mean temperature and transformed Eulerian stream function χ and related mean meridional circulation (v*,w*) above the tropical tropopause, both with each other and with respect to the CONTROL experiment. The climatological annual mean differences of zonal mean T, χ, and w* between W-QBO and E-QBO are displayed in Figure 8. The tropopause temperature signal is positive between 15°S and 15°N and reaches 0.7 K at the equator at 100 hPa. The maximum of 3.5 K occurs at the equator at 50 hPa. Weaker negative values are found north and south of the main warming and extend from 50 hPa downward. The warm-cold-warm pattern at 30 hPa belongs to the upper portion of the secondary meridional circulation.

The implied mass fluxes are shown by the TEM stream function in Figure 8b. The eastward phase of the QBO, as assimilated permanently in W-QBO, forces equatorial downward fluxes of 15.4×10^8 kg/s, 12.4×10^8 kg/s and 20.2×10^8
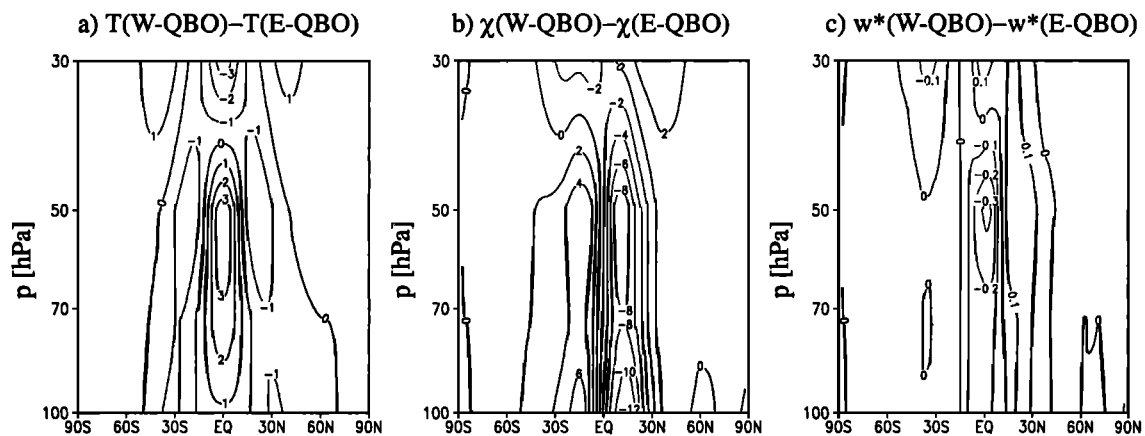

Figure 8. Differences of the climatological annual means in W-QBO and E-QBO of (a) zonal mean temperature in K, (b) transformed Eulerian mean stream function χ in 10^8 kg/s, and (c) w* in mm/s.

kg/s at 50 hPa, 70 hPa, and 100 hPa with respect to the westward QBO phase in E-QBO. Here it is surprising to find that the downward flux decreases first between 50 hPa and 70 hPa, but is strongly reinforced between 70 hPa and 100 hPa, indicating the potential of a positive feedback of the tropospheric circulation near the tropical tropopause to the QBO-driven perturbations. This has to be compared with the QBO signal of tropical downward mass flux at 100 hPa estimated by *Seol and Yamazaki* [1998]. They analyzed NCEP daily analysis of the period December 1988 to November 1995 and found a peak to peak amplitude of 26×10^8 kg/s. Thus the model-determined value is 22% less than the analyzed value. This represents a reasonable agreement between the modeled and the analyzed value, remembering that the assimilated QBO was 75% of the prescribed QBO. The streamfunction in Figure 8b shows further an asymmetry between the hemispheres. The QBO-forced upwelling at the equator at 50 hPa partitions into 62% northward flow and 38% southward flow. Hemispheric asymmetries in the strength of the QBO secondary meridional circulation were diagnosed indirectly by *Randel et al.* [1998] in their analysis of interannual anomalies of H_2O and CH_4. They investigated QBO-related signals in these tracers as measured by HALOE between November 1991 and March 1997, covering two to three cycles of the QBO. In the NH they found a QBO-related variability of H_2O and CH_4 at 10 hPa that is significantly stronger than in the SH. Additionally they showed a corresponding plot of w* at 10 hPa, analyzed in United Kingdom Meteorological Office (UKMO) analyses, which shows the same kind of hemispheric asymmetries in variability coherent with the QBO. Figure 8c shows the difference pattern of w* in W-QBO and E-QBO. The signal is concentrated strongly at the equator, where it has a maximum relative sinking of -0.33 mm/s at 50 hPa. The relative upwelling is strongest in the Northern Hemisphere, where it has a peak value of 0.19 mm/s at 50 hPa.

The annual zonal mean difference of the tropopause temperature (Figure 8a) is a conservative estimate of the QBO temperature effect on the water vapor in the lower stratosphere, because there is no discrimination of favorable or unfavorable ambient conditions for STE. Further, the relationship between temperature change and moisture change depends also on the absolute temperature, assuming the air is saturated. A potential selection criterion for the dry air ascent to the stratosphere, which is produced in January, is the local climatological mean humidity at the tropopause, assuming that air enters the equatorial stratosphere necessarily in the driest places, independent of the QBO phase. The climatology of q_{E-QBO} and the difference fields $T_{W-QBO} - T_{E-QBO}$ and $q_{W-QBO} - q_{E-QBO}$ at 100 hPa in January are shown in Figure 9. The driest air is found over the equatorial western Pacific, where the mixing ratio is less than 4 ppmv, and the minimum value obtained is 2.7 ppmv. The highest values are found east of the continents along 30°S, attaining values up to 7.5 ppmv. Similar high-moisture areas exist in the boreal summer season along 30°N (not shown). The temperature signal (Figure 9b) exhibits the typical zonal structure of positive values between 15°S and 15°N and neg-

ative values in the subtropics along 30°latitude, as expected from the opposite QBO forcing in W-QBO and E-QBO (cf. Figure 8a). In the equatorial latitudes the relative warming exceeds 1 K between 90°E and 170°E. Maximum values are above 1.5 K. The high values in the northern high latitudes are caused by internal variability. The moisture differences are quite uniform poleward of 30°latitude, where the
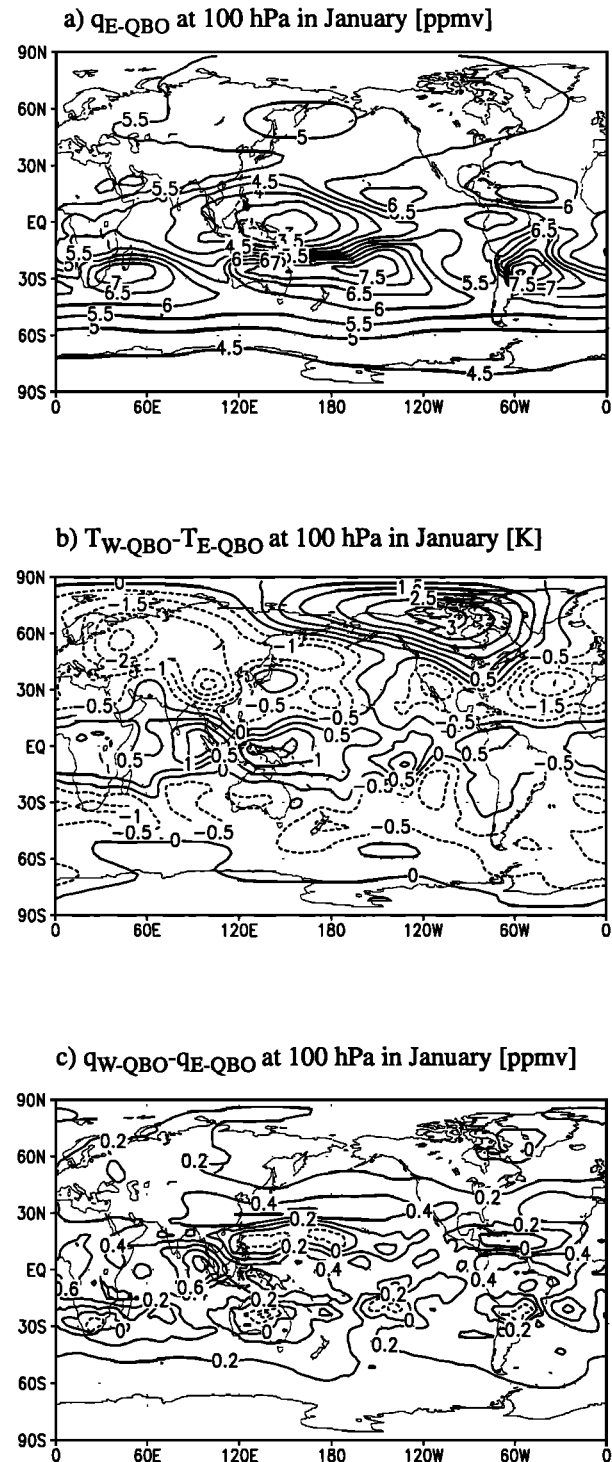
a) q_{E-QBO} at 100 hPa in January [ppmv]

b) T_{W-QBO}-T_{E-QBO} at 100 hPa in January [K]

c) q_{W-QBO}-q_{E-QBO} at 100 hPa in January [ppmv]

Figure 9. January climatology of (a) q_{E-QBO} in ppmv, (b) $T_{W-QBO} - T_{E-QBO}$ in K, and (c) $q_{W-QBO} - q_{E-QBO}$ in ppmv at 100 hPa.

Table 2. Climatological Temperature and Humidity Differences W-QBO-E-QBO at 100 hPa in Areas Where q_{E-QBO} Is Less Than the Specified q_{max} for January

q_{max}, ppmv	ΔT_{W-E}, K	Δq_{W-E}, ppmv
3.0	1.39	0.55
3.5	1.11	0.47
4.0	0.81	0.40
4.5	0.73	0.40

100 hPa level is in the stratosphere, but resembles the temperature pattern toward the equator (Figure 9c). The equatorial region where ΔT is greater than 1 K shows typical values of 0.4 ppmv or higher. Negative values occur along 30°S, where the full field has areas of high humidity (Figure 9a), and along 20°N in the western Pacific. The climatological fields of the other months have the same characteristics, warm/moist differences along the equator and cold/dry differences in banded structures between 15° and 30° latitude in areas of high moisture contents.

Table 2 contains QBO induced temperature and humidity differences W-QBO−E-QBO averaged over selected areas in Figure 9b and Figure 9c, where the climatological January mean humidity does not exceed a certain humidity threshold q_{max} in E-QBO (Figure 9a). This selection criterion results in ranges of 0.73 K to 1.39 K and 0.40 ppmv to 0.55 ppmv for q_{max} between 4.5 ppmv and 3.0 ppmv. This means that the QBO causes a tropopause temperature signal of approximately 1 K in the assumed primary area of dry air production, causing a QBO-explained signal in tropopause humidity of 0.40 ppmv to 0.55 ppmv, which is an upper estimate for a QBO signal in the dry phase of the atmospheric tape recorder. The upward propagation velocity, that is, the tape speed, is also modified by the QBO (Figure 8b).

The experiments W-QBO and E-QBO have constant QBO phases for the whole duration. Hence the warmer/moister and cooler/drier conditions at the equatorial tropopause, enforced by the assimilated QBO phases in W-QBO/E-QBO, persist also over the whole length of the integrations. Because W-QBO and E-QBO have been started originally from the same initial states as CONTROL, including the same stratospheric humidity fields, the humidity fields in W-QBO and E-QBO will show sustained positive and negative humidity trends in the stratosphere with respect to CONTROL. Eventually, the experiments would find new equilibria, dependent on the phase-locked QBO states. The equilibration timescale is also likely to depend on the QBO phase, since w^* differs also between the experiments.

The overall effect on the equatorial specific humidity is shown in Figure 10. It shows time series of the zonal mean specific humidity at 50 hPa averaged from 10°S to 10°N, smoothed by a running mean over 12 months for W-QBO, E-QBO, and CONTROL. Due to the long timescales of tracer transport in the stratosphere, the equilibration of water vapor at 50 hPa is not yet completed, in spite of a 10 year initialization run at the beginning of the CONTROL exper-

iment, resulting in a small positive drift. This slow equilibration is a typical problem in modeling the distributions of stratospheric trace constituents [*Mote*, 1995]. The average over the last year is 0.37 ppmv, or 7.7% higher than the average over the first year of CONTROL. The linear trend is +0.032 ppmv/yr. However, with respect to the CONTROL, the time series of the perpetual QBO phase experiments W-QBO and E-QBO have a significant positive and negative trend, respectively. In the former case of a perpetual eastward QBO phase, the smoothed specific humidity increases steadily at a rate of 0.047 ppmv/yr until it levels off after 9 years, probably approaching a new equilibrium. In the latter case of a perpetual westward QBO phase, the specific humidity seems to be close to an equilibrium and there is no significant trend. Because the final climatological value of the specific humidity in W-QBO is unknown, it is only possible to conclude that the climatological difference in the annual mean specific humidity at 50 hPa at the equator is at least 0.40 ppmv or some 10% higher in the limiting case of a perpetual eastward QBO phase than in the opposite case. Moreover, the result also suggests that the time to reach equilibration has a much longer timescale than the QBO. On the basis of the perpetual QBO phase experiments, the QBO signal (of a realistically evolving QBO) may be expected to lie in the range of 0.05 to 0.08 ppmv.

The meridional structure of the difference field of moisture in W-QBO and E-QBO is shown in Figure 11. Figure 11a contains the difference pattern of the first year, for which one may assume that the field represents the annual mean perturbation with respect to the common initial state of W-QBO and E-QBO. The main features of the first year difference are a positive difference at the equator and negative anomalies near 20°N and 20°S. The negative signals are essentially restricted to 100 hPa, showing the year 1 zonal mean tropopause differences, which are colder/drier at these latitudes. The equatorial warm signal rises to nearly 50 hPa.
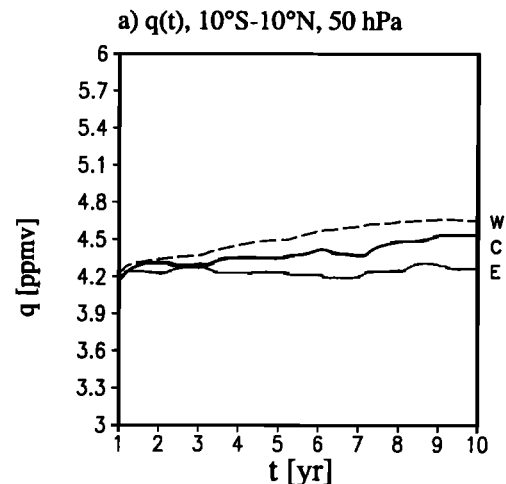
a) q(t), 10°S-10°N, 50 hPa

Figure 10. One year running average time series of specific humidity in ppmv averaged between 10°S and 10°N at 50 hPa in CONTROL (C, thick solid curve), W-QBO (W, long-dashed curve) and E-QBO (E, thin solid curve).
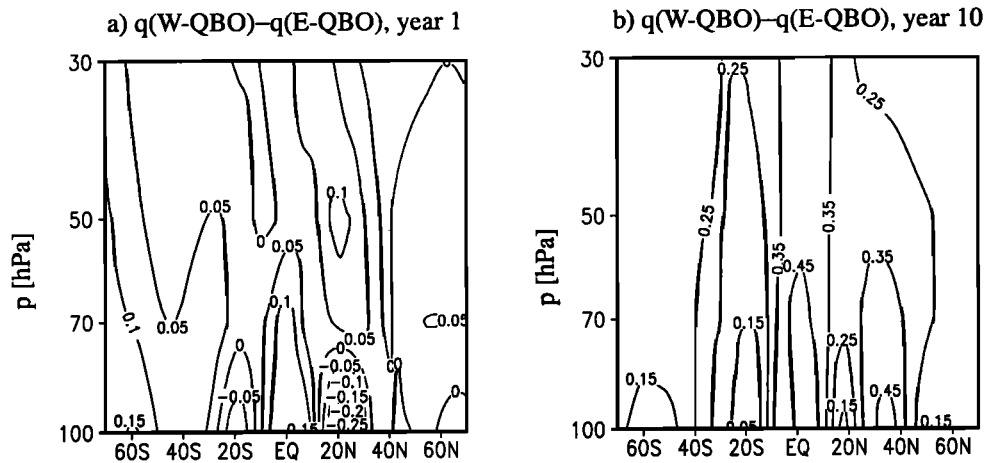
Figure 11. Difference of specific humidity averaged over (a) year 1 and (b) year 10 in W-QBO and E-QBO in ppmv.

The differences poleward of 40°latitude are dominated by internal variability. Thus the moisture forcing in W-QBO with respect to E-QBO, which is effective at 100hPa, consists of net moisture injection near the equator and net removal near 20°N and 20°S.

Figure 11b shows the difference field averaged over the last year, when both experiments are presumably close to their new equilibria. The values are positive everywhere, as expected since the equatorial "cold traps" in W-QBO are systematically warmer than in E-QBO, leading to an ongoing replacement of old dry air by newer and moister air. At the equator the stratospheric air is moistened by almost uniform 0.45 ppmv. This value is close to the upper estimate found above. As the vertical gradient is now very small, lateral loss of moisture across the almost vertical 0.35 ppmv isolines must be balanced by higher upward moisture transport across the equatorial tropopause.

Two minima of 0.05 ppmv and 0.10 ppmv are found near 20°S and 20°N at 100 hPa, both increasing with height. These minima have positive values compared to negative values in the year 1 difference plot. However, the vertical gradient did not change, indicating strong meridional mixing at 100 hPa. Additionally there are two positive maxima of 0.28 ppmv and 0.51 ppmv near 35°S and 35°N, respectively. These have not been resolved in the first year difference pattern. Obviously the stratosphere is also moistened at these latitudes, and these sources are remarkably different in strengths, weak in the SH and strong in the NH. It is likely that this is related to the different strength in eddy activity in both hemispheres, but this question will not be investigated further here.

5.2. Realistically Evolving QBO

This section describes the sensitivity of the temperature, vertical transport, and specific humidity in the equatorial lower stratosphere to ENSO and QBO as was found in the experiments AMIP and AMIP-QBO. Results are shown for monthly mean variables averaged from 10°N to 10°S, where the annual cycle is suppressed by a running mean over 12

months. Interannual signals of temperature and vertical transport are computed as the difference of the smoothed time series to the temporal average of the total time series. In the case of specific humidity one has to subtract a linear trend also.

The interannual signals of T and w* are displayed in the left and right column, respectively, of Figure 12. The upper, middle and lower rows contain the signals in AMIP and AMIP-QBO and the signal differences AMIP-QBO−AMIP. The time axis indicates the first month of a running mean over 12 months.

The interannual temperature signal in AMIP (Figure 12a) has no vertical tilt. The amplitudes are in the range of −1.2 K to +0.8 K and obtain the extrema at 70 to 50 hPa. Cold signals occur in 1982-1983, 1986-1987, and toward the end of the experiment in 1992. Warm events occur in 1980-1981, 1983-1984, and 1990. The sequence of warm and cold interannual anomalies coincides with the series of El Niño and La Niña events. It is highly probable that the prescribed observed SSTs are indeed the forcing mechanism of these anomalies. However, it is hardly possible to validate the anomalies directly by analyzed data because of the relatively small amplitudes of the signals in AMIP in comparison to the temperature anomalies caused by the QBO and the volcanic eruptions of El Chichón (April 1982) and Mount Pinatubo (June 1991) in the real atmosphere. Also the signal of the vertical transport w* in AMIP (Figure 12b) has no vertical tilt. Sinking and rising motions occur when the temperature signal is negative and positive, respectively. The values are, in general, in the range of −5 to +5 m/d, except in 1982-1983, when the sinking motion reaches 10 m/d at 70 hPa and exceeds 12.5 m/ d at 100 hPa. The signal in w* is strongest at 100 hPa, that is, it is caused by tropospheric processes.

Figure 12c and Figure 12d show the corresponding panels of the experiment AMIP-QBO. Here we have external forcings by the prescribed SST and at the same time by the assimilated QBO. The obtained interannual signals of T and w* exhibit the typical QBO pattern of descending phases,

but there are also major disturbances of these patterns, for example, in 1982-1983 and 1988-1989, when the ENSO effects in T and w* cancel the QBO-forced downward progression of warm / downward and cold / upward signals, re-spectively. In other years the ENSO signal strengthens the QBO-given pattern, for example, the cold signal in 1981-1982 or the warm signal in 1987-1988. In general, the T and w* signals in AMIP-QBO resemble a linear superposition
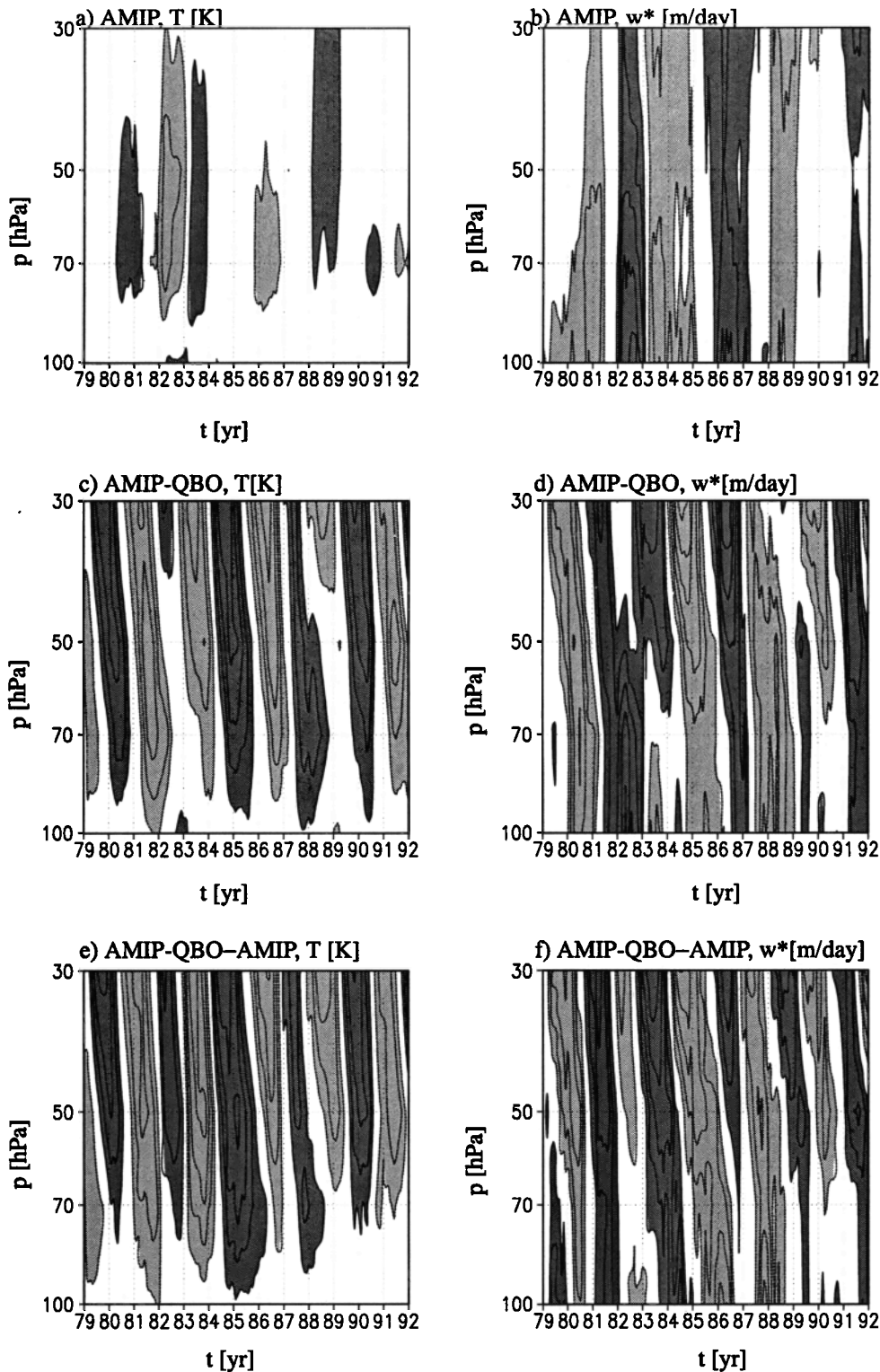

Figure 12. Interannual signals of (a) T and (b) w* averaged from 10°S to 10°N in the experiment AMIP. Similar data are shown for (c) T and (d) w* in AMIP-QBO. The difference of the signals in AMIP-QBO and AMIP is shown for (e) T and (f) w*. Isoline distances are 0.5 K and 2.5 m/day for T and w*, respectively. Dark and light shading indicates positive and negative values; the 0 -line is suppressed.

of a QBO-signal and an ENSO signal. Hence a subtraction of the ENSO induced signals in AMIP (cf. Figures 12a and 12b) from those in AMIP-QBO results in signals shown in Figure 12e and Figure 12f, exhibiting a very clear QBO pattern, and the deviations from an imaginary pure QBO pattern are considerably smaller than in Figure 12c and Figure 12d. However, below 70 hPa the QBO influences are strongly decreasing and there are considerable disturbances due to non-linear contributions by the ENSO forcing and/or internal tropospheric variations.

AMIP-QBO is the most complete experiment in the experimental design of Table 1. It includes the QBO as well as the observed SST fields. Therefore it is of interest to compare the temperature anomalies of AMIP-QBO with those derived from observations as done here for the ECMWF reanalysis (ERA) data [*Gibson et al.*, 1997]. Before discussing the figures it is necessary to recall the volcanic eruptions of El Chichón in April 1982 and Mount Pinatubo in 1991. These events caused temperature disturbances in the stratosphere (warming) as well as in the troposphere (cool-

ing) due to the direct effect of radiative forcing by the volcanic aerosols which were injected to the lower stratosphere [*Stendel and Bengtsson*, 1996]. This forcing is completely neglected in the GCM experiments, and it has to be expected that the temperature disturbances in AMIP-QBO and in ERA are in disagreement in 1982-1983 and 1991-1992. For this reason the temperature perturbation in ERA is computed with respect to the climatological mean temperature of the years 1979-1981 and 1984-1990, instead of the full time series, and shown in Figure 13a. The ERA temperature anomalies confirm that AMIP-QBO follows closely the observed anomalies during years unaffected by the volcanic aerosols. The sequence of cold-warm-cold anomalies starting at 30 hPa in 1983 propagate down to the tropopause. They are followed by an initially weak warm anomaly with an almost detached maximum value attained at 70 hPa in 1988, which blocks the descent of a cold anomaly from above. Clear differences occur from 1981 to 1983. The ERA show a very weak cold anomaly followed by a very intense warm anomaly that is almost connected to the pre-
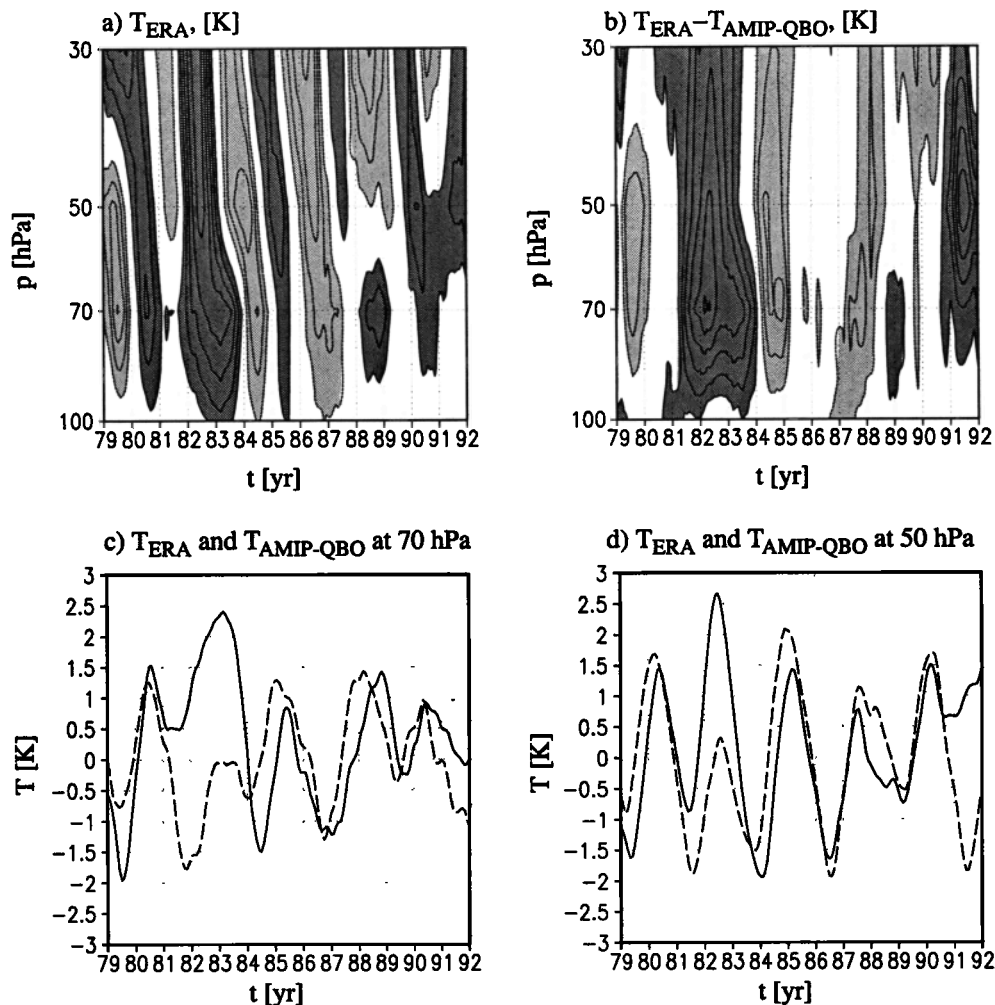

Figure 13. (a) Interannual anomalies of T averaged from 10°S to 10°N in ECMWF reanalysis data (ERA). (b) Difference plot of T anomalies in ECMWF reanalysis and experiment AMIP-QBO (cf. Figure 6c). Isoline distances are 0.5 K, dark and light shading indicates positive and negative values, and the 0 -line is suppressed. (c) Temperature time series in ERA and AMIP-QBO at 70 hPa. (d) Temperature time series in ERA and AMIP-QBO at 50 hPa.
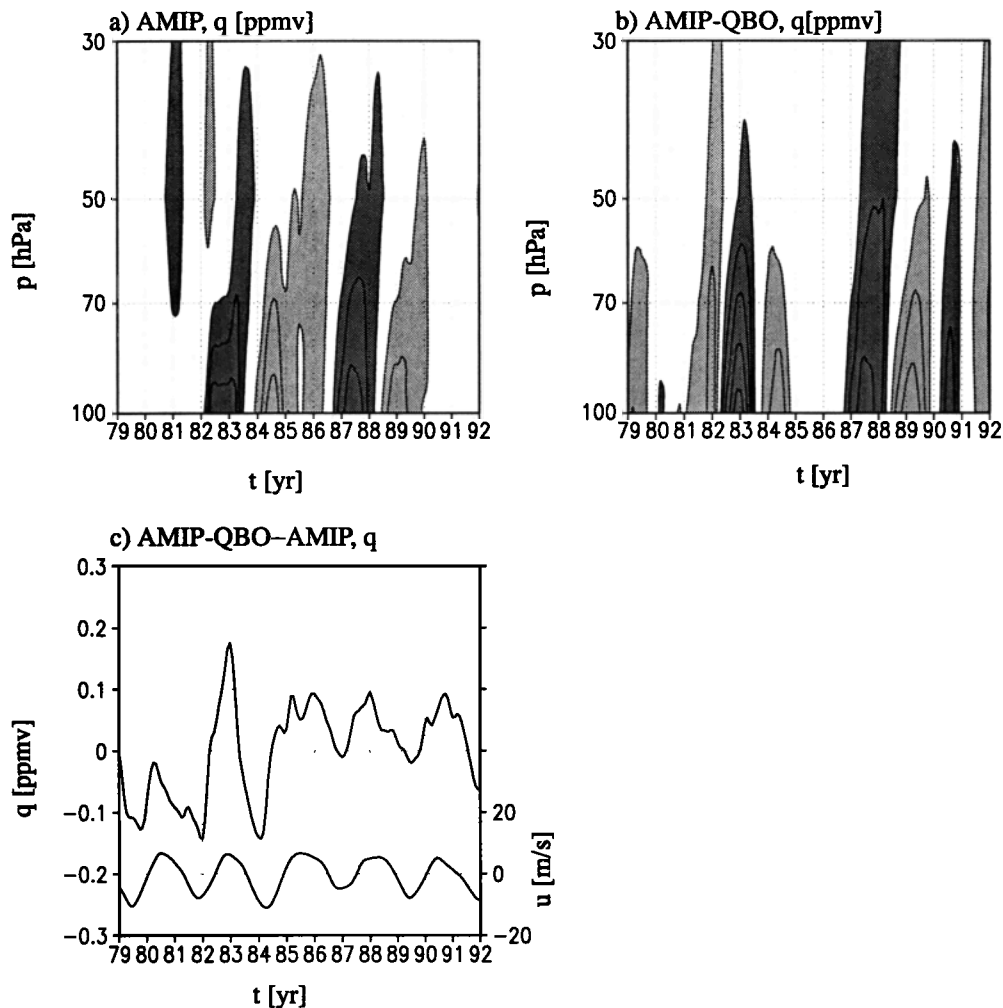
Figure 14. (a and b) Interannual signals of the specific humidity q averaged from 10°S to 10°N in the experiments AMIP and AMIP-QBO. Isoline distances are 0.1 ppmv. Dark and light shading indicates positive and negative values, and the 0 -line is suppressed. (c) Signal difference AMIP-QBO—AMIP at 50 hPa together with the equatorial zonal wind at 50 hPa smoothed like the humidity by a 1 year running mean.

ceding warm anomaly at 70 hPa, while AMIP-QBO shows a strong cold anomaly followed by a weak, almost non existent warm anomaly. Similarly, in 1991 the cold anomaly in ERA is very small and superseded by a warm anomaly connected to the previous warm anomaly, while AMIP-QBO shows a well-developed cold anomaly. These differences are direct effects of the volcanic aerosol deposited in the lower stratosphere. Their warming effect is comparable to the QBO-induced temperature anomalies, as demonstrated in Figure 13b, which shows the difference of the temperature anomalies in ERA (cf. Figure 13a) and AMIP-QBO (cf. Figure 12c). The differences have maxima of 2.5 K centered at 70 to 50 hPa after El Chichón and at 50 hPa after Mount Pinatubo. These values are in good agreement with observed warmings of the tropical lower stratosphere due to major volcanic eruptions [*Labitzke and McCormick,* 1992; *Angell,* 1997]. A direct comparison of the ERA and AMIP-QBO temperature time series at 70 hPa and 50 hPa is given in Figure 13c and Figure 13d, respectively. At both levels, the major differences occur after the eruptions of El Chichón

and Mount Pinatubo. The disagreement of AMIP-QBO with ERA is sufficiently explained by the neglect of the volcanic events in AMIP-QBO. For the other years the interannual temperature anomalies of the experiment are realistic with respect to the ERA data.

The interannual signal in the specific moisture q is displayed in Figure 14. Figures 14a and 14b show the signals found in the experiments AMIP and AMIP-QBO, while Figure 14c shows the difference plot of AMIP-QBO—AMIP. The main feature in Figure 14a and Figure 14b is the upward propagation of alternating positive and negative deviations. In AMIP, the El Niño episodes in 1982 and 1987 cause two positive anomalies, which are followed by two negative anomalies during the La Niña phases. At 50 hPa the moisture is about 0.25 ppmv higher after El Niño than after La Niña. Weaker deviations of both signs occur mainly between 50 hPa and 30 hPa. In AMIP-QBO, the signal shows primarily a disturbed QBO pattern. Positive signals propagate upward from 100 hPa in 1980, 1982-1983, 1985, 1987-1988, and 1990, although their strength varies considerably.

The positive signals are strongest after the El Niño events and weakest in the year 1985, which is due to the La Niña of that year. Thus the pattern reflects an interference of QBO- and ENSO-related influences. A difference plot of the signals in q in the experiments AMIP-QBO and AMIP is shown in Figure 14c for the 50 hPa level. This panel contains also the time series of the equatorial zonal wind at 50 hPa, that is, of the QBO, smoothed by a 1 year running mean. The curve of the specific humidity clearly demonstrates the occurrence of a QBO-induced signal in the specific humidity. However, there is also a long-term modulation in the sense that the curves have an almost steplike increase of approximately 0.15 ppmv from the years 1982 to 1985, which is of the same order of magnitude as the amplitude of the single oscillations before 1982 and after 1985, which is in the range of 0.1 to 0.15 ppmv. The QBO signal reaches 50% of the ENSO signal in humidity at 50 hPa. The modeled value is certainly a lower estimate of the QBO signal in real equatorial moisture at 50 hPa due to the problems related to the coarse resolution of the model stratosphere (cf. section 4). The ratio of this model-estimated QBO amplitude to the modeled annual cycle of moisture is 14% to 21%.

Figure 15 shows the observed humidity in the same latitude belt of 10°S to 10°N at 50 hPa for the years 1992 to 1998, as measured by the HALOE instrument on the UARS satellite [Dessler at al., 1998]. This time series is considerably shorter than the model time series, and it has gaps when the orbit did not allow measurements within these latitudes. The data were averaged over single sweeps of the orbit, resulting in approximately one data value per month. Because of the relatively short record, the data are shown without further processing, except for the averaging over the equatorial latitudes. Data before 1993 are badly contaminated by the eruption of Mount Pinatubo in June 1991, but are shown for completeness. The lower frequency of measurements after 1995 is related to problems with the electrical power supply on UARS.

A subjective analysis of the (broken) curve may suggest that there is indeed a quasi-biennial behavior. The local max-
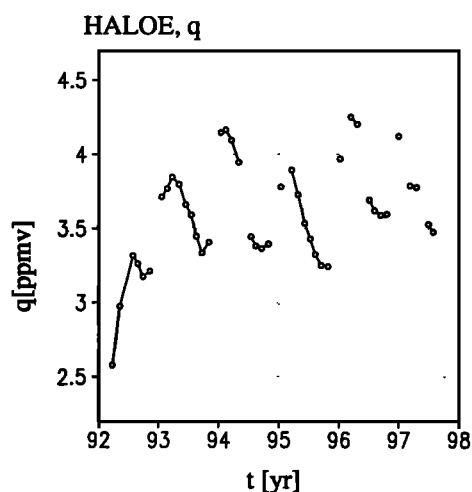
HALOE, q

Figure 15. Water vapor measured by HALOE at 50 hPa, averaged from 10°S to 10°N.

ima of the years 1994 and 1996 are 0.2 to 0.3 ppmv higher than those of the preceding years 1993 and 1995. The timing is coincident with the QBO phase of these years and has the same phase relationship as the model signal to its prescribed QBO. The seasonal cycle has an amplitude of about 0.8 ppmv [Randel et al., 1998]. If the difference of 0.2 to 0.3 ppmv were taken as the real QBO signal in the water vapor mixing ratio at this level, then it would be double the signal in the model, indicating again mixing and diffusivity problems related to the coarse model resolution. However, the model is able to create interannual peak to peak differences of at least 0.3 ppmv, as seen in the 1983 peak in Figure 14. Additionally, the evolution of the specific humidity in AMIP-QBO is a nice example of how the combination of two forcings at different timescales can cause low-frequency variability. After the step-like increase the QBO signal remains until the end of the experiment on the upper level. This duration of 7 years is considerably longer than the typical space between El Niños in the years 1979 to 1992 and in any event longer than the mean QBO period.

6. Conclusions

This study uses data from a set of GCM experiments to study the influences of the QBO on the fields of temperature, vertical transport, and specific humidity in the equatorial lower troposphere. The set of experiments consists of a control experiment with neither interannual SST variations nor QBO, an AMIP experiment with interannual SST variations following observations from 1979 to 1992, two experiments including perpetual eastward and westward QBO phases without interannual SST variations, and an AMIP-like experiment including additionally the QBO as observed in 1979 to 1992. The QBO was assimilated by a linear relaxation scheme acting on the zonal wind in the QBO domain.

The comparison of W-QBO and E-QBO shows that the GCM successfully generates the QBO secondary meridional circulation in terms of strength of the equatorial mass flux at 100 hPa (20×10^8 kg/s) and amplitude of the adiabatic temperature in the QBO domain (3.5 K). The potential change in moisture at the driest (since coldest) areas of the tropical tropopause is estimated to be in the range of 0.40 ppmv to 0.55 ppmv. After 10 years of integration the moisture content in the equatorial stratosphere is nearly equilibrated in both experiments, resulting in a difference of 0.45 ppmv. The first-year difference pattern indicates an underestimation of the humidity QBO signal to be found in AMIP-QBO due to exaggerated dilution related to the coarse resolution.

The comparison of AMIP, AMIP-QBO, and ECMWF reanalysis (ERA) confirms again the ability of the model to set up a realistic secondary meridional circulation and hence a QBO temperature signal. The subtraction of the interannual variability of temperature in AMIP, due to ENSO, from that in AMIP-QBO results in a smooth QBO pattern. Differences between AMIP-QBO and ERA are well explicable by the volcanic eruptions of El Chichón and Pinatubo. The interannual variability of the stratospheric equatorial humidity is marked by upward propagating anomalies emanat-

ing from the tropopause. This happens in AMIP on ENSO timescales. El Niño and La Niña episodes are followed by moister and drier anomalies, respectively. The ENSO variability explains differences of approximately 0.25 ppmv at 50 hPa. AMIP-QBO generates rising anomalies resembling the ENSO pattern after strong El Niño or La Niña events, but varying on the QBO timescale elsewhere. The difference of AMIP-QBO and AMIP indicates a QBO amplitude of 0.1 ppmv to 0.15 ppmv at 50 hPa, equivalent to 50% of the ENSO-explained amplitude. This amplitude is indeed smaller than the upper estimate of 0.45 hPa, found after approximate equilibration in W-QBO and E-QBO. Further, the humidity difference AMIP-QBO−AMIP contains considerable low-frequency variability resulting from interferences of ENSO and QBO timescales. These have the same magnitude as the QBO signal. The upward propagation of the humidity anomalies in AMIP and AMIP-QBO is too fast. This deficiency is caused by the coarse vertical resolution of the model.

The comparison with HALOE measurements of humidity at 50 hPa confirms the signals found in the model. One finds a quasi-biennial variation in the years 1993 to 1996 corresponding to the QBO of these years. However, the time series is quite short to be used as a rigorous tool of validation for QBO timescales.

Finally, the results of these experiments encourage the use of the QBO assimilation in model experiments focusing on the transport, temperature, and humidity variability in the tropical lower stratosphere.

References

Andrews, D. G., J. R. Holton, and C. B. Leovy, *Middle Atmosphere Dynamics*, 498 pp., Academic, San Diego, Calif., 1987.

Angell, J. K., Stratospheric warming due to Agung, El Chichón, and Pinatubo taking into account the quasi-biennial oscillation, *J. Geophys. Res., 102*, 9479-9485, 1997.

Balachandran, N. K., and D. Rind, Modeling the effects of UV variability and the QBO on the troposphere-strato- sphere system, I, The middle atmosphere, *J. Clim., 8*, 2058-2079, 1995.

Brinkop, S., and E. Roeckner, Sensitivity of a general circulation model to parameterizations of cloud-turbulence interactions in the atmospheric boundary layer, *Tellus, 47A*, 197-220.

Cordero, E. C., S. R. Kawa, and M. R. Schoeberl, An analysis of tropical transport: Influence of the quasi-biennial oscillation, *J. Geophys. Res., 102*, 16453-16461, 1997.

Dessler, A. E., M. D. Burrage, J.-U. Grooss, J. R.Holton, J. L. Lean, S. T. Massie, M. R. Schoeberl, A. R. Douglass, and C. H. Jackman, Selected science highlights from the first 5 years of the Upper Atmosphere Research Satellite (UARS) program, *Rev. Geophys., 36*, 183-210, 1998.

Dunkerton, T. J., and D. P. Delisi, Climatology of the equatorial lower stratosphere, *J. Atmos. Sci., 42*, 376-396, 1985.

Fouquart, Y., and B. Bonnel, Computations of solar heating of the Earth's atmosphere: A new parameterization, *Beitr. Phys. Atmos., 53*, 35-62, 1980.

Gibson, J. K., P. Kållberg, S. Uppala, A. Hernandez, A. Nomura, and E. Serrano, ERA description, *ECMWF re-analysis project report series, 1*, 72 pp., Eur. Cent. for Medium-Range Weather Forecasts, Shinfield Park, Reading, England, 1997.

Hamilton, K., Interannual variability in the Northern Hemisphere winter middle atmosphere in control and perturbed experiments with the GFDL SKYHI general circulation model, *J. Atmos. Sci., 52*, 44-66, 1995.

Haynes, P. H., C. J. Marks, M. E. McIntyre, T. G. Shepherd, and K. P. Shine, On the "down- ward control" of extratropical diabatic circulations by eddy-induced mean zonal forces, *J. Atmos. Sci., 48*, 651-678, 1991.

Holton, J. R., P. H. Haynes, M. E. McIntyre, A. R. Douglass, R. B. Rood, and L. Pfister, Stratosphere-troposphere exchange, *Rev. Geophys., 33*, 405-439, 1995.

Kalnay E., et al., The NCEP/NCAR 40-year reanalysis project, *Bull. Am. Meteorol. Soc., 77*, 437-471, 1996.

Kley, D., E. J. Stone, W. R. Henderson, J. W. Drummond, W. J. Harrop, A. L. Schmeltekopf, T. L. Thompson, and R. H. Winkler, In situ measurements of the mixing ratio of water vapor in the stratosphere, *J. Atmos. Sci., 36*, 2513-2524, 1979.

Kodera, K., M. Chiba, and K. Shibata, A general circulation model study of the stratospheric circulation during the Northern Hemisphere winter, *Geophys. Res. Lett., 18*, 1209-1212, 1991.

Krishnamurti, T. N., J. Xue, H. S. Bedi, K. Ingles, and D. Oosterhof, Physical initialization for numerical weather prediction over the tropics, *Tellus, 43AB*, 53-81, 1990.

Labitzke, K., and M. P. McCormick, Stratospheric temperature increases due to Pinatubo aerosols, *Geophys. Res. Lett., 19*, 207-210, 1992.

Miller, M. J., T. N. Palmer, and R. Swinbank, Parameterization and influence of sub-grid scale orography in general circulation and numerical weather prediction models, *Meteorol. Atmos. Phys., 40*, 84-109, 1989.

Morcrette, J.-J., L. Smith, and Y. Fouquart, Pressure and temperature dependence of the absorption in longwave absorption parameterization, *Beitr. Phys. Atmos. 59*, 455-469, 1986.

Mote, P. W., The annual cycle of stratospheric water vapor in a general circulation model, *J. Geophys. Res., 100*, 7363-7379, 1995.

Mote, P. W., K. H. Rosenlof, M. E. McIntyre, E. S. Carr, J. C. Gille, J. R. Holton, J. S. Kinnersley, H. C. Pumphrey, J. M. Russell III, and J. W. Waters, An atmospheric tape recorder: The imprint of tropical tropopause temperature on stratospheric water vapor, *J. Geophys. Res., 101*, 3989-4006, 1996.

Naujokat, B., An update of the observed quasi-biennial oscillation of the stratospheric winds over the tropics, *J. Atmos. Sci., 43*, 1873-1877, 1986.

Newell, R. E., and S. Gould-Stewart, A stratospheric fountain?, *J. Atmos. Sci., 38*, 2789-2796, 1981.

Nordeng, T. E., Extended versions of the convective parameterization scheme at ECMWF and their impact on the mean and transient activity of the model in the tropics. *ECMWF Research Department Technical Memorandum No. 206*, 41 pp., Eur. Cent. for Medium-Range Weather Forecasts, Reading, England, 1996.

Pawson, S., and M. Fiorino, A comparison of reanalyses in the tropical stratosphere, 1, Thermal structure and the annual cycle, ERA description, *Clim. Dyn., 14*, 631-644, 1998a.

Pawson, S., and M. Fiorino, A comparison of reanalyses in the tropical stratosphere, 2, The quasi-biennial oscillation, ERA description, *Clim. Dyn., 14*, 645-658, 1998b.

Pawson, S., K. Labitzke, R. Lenschow, B. Naujokat, B. Rajewski, M. Wiesner, and R.-C. Wohlfart, Climatology of the Northern Hemisphere stratosphere derived from Berlin analyses, I, Monthly means, *Meteorol. Abhandlungen, Ser. A Monogr.*, Vol.

7, part 3, 299 pp., Verlag von Dietrich Reimer, Berlin, Germany, 1993.

Randel, W. J., and Fei Wu, Isolation of the ozone QBO in SAGE II data by singular-value decomposition, *J. Atmos. Sci., 53,* 2546-2559, 1996.

Rockel, B., E. Raschke, and B. Weyres, A parameterization of broad band radiative transfer properties of water ice and mixed clouds, *Beitr. Phys. Atmos., 64,* 1-12, 1991.

Roeckner, E., Parameterization of cloud radiative properties in the ECHAM4 model. *WMO/TD-No. 713, WCRP-Report No. 90,* 105-116, 1995.

Roeckner, E., K. Arpe, L. Bengtsson, M. Christoph, M. Claussen, L. Dümenil, M. Esch, M. Giorgetta, U. Schlese, and U. Schulz-weida, The atmospheric general circulation model ECHAM-4: Model description and simulation of present day climate, *Rep. 218,* 90 pp., Max-Planck-Inst für Meteorol., Hamburg, Germany, 1996.

Rosenlof, K. H., A. F. Tuck, K. K. Kelly, J. M. Russell III, and M. P. McCormick, Hemispheric asymmetries in water vapor and inferences about transport in the lower stratosphere, *J. Geophys. Res., 102,* 13213-13234, 1997.

Seol D.-I., and K. Yamazaki, QBO and Pinatubo signals in the mass flux at 100 hPa and stratospheric circulation, *Geophys. Res. Lett., 25,* 1641-1644, 1998.

Stendel, M., and L. Bengtsson, Monitoring the temperature of the troposphere by means of a general circulation model, *Rep. 186,* 26 pp., Max-Planck-Inst. für Meteorol., Hamburg, Germany, 1996.

Sundquist, H., A parameterization scheme for non-convective condensation including prediction of cloud water content, *Q. J. R. Meteorol. Soc., 104,* 677-690, 1978.

Sundqvist, H., E. Berge, and J. E. Kristjansson, Condensation and cloud parameterization studies with a mesoscale numerical weather prediction model, *Mon. Weather Rev., 117,* 1641-1657, 1989.

Tiedtke, M., A comprehensive mass flux scheme for cumulus parameterization in large scale models. *Mon. Weather Rev., 117,* 1779-1800, 1989.

Tung, K. K., and H. Yang, Global QBO in circulation and ozone, I, Reexamination of observational evidence, *J. Atmos. Sci., 51,* 2699-2707, 1994.

Williamson, D. L., and P. J. Rasch, Water vapor transport in NCAR CCM2, *Tellus, 46A,* 34-51, 1994.

L. Bengtsson and M. A. Giorgetta, Max-Planck-Institute for Meteorology, Bundesstr. 55, D-20146 Hamburg, Germany, (e-mail: bengtsson@dkrz.de; giorgetta@ dkrz.de)